Int J Adv Manuf Technol (2015) 78:177–187
DOI 10.1007/s00170-014-6621-x

ORIGINAL ARTICLE

Warpage optimization with dynamic injection molding technology and sequential optimization method

Xinyu Wang · Junfeng Gu · Changyu Shen · Xicheng Wang

Received: 12 May 2014 / Accepted: 23 November 2014 / Published online: 5 December 2014

Abstract Warpage is one of the serious defects for thin wall plastic injected component. This paper employs dynamic filling and packing process parameters as the new design variables to perform the optimization on warpage for the first time. In this paper, several numerical implementations for dynamic filling and packing are discussed in detail. The unclear functional relationship between the objective (maximum warpage) and 12 process parameters is characterized by the Kriging surrogate model approximately. These process parameters not only include the conventional process parameters, like melt temperature, filling time, packing pressure etc., but also include the new dynamic process parameters involving amplitude, frequency, and phase of vibration. Subsequently, the efficient global optimization method (expected improvement-based method) is used for searching the optimum solution sequentially. Final results suggest a set of process parameters of the dynamic injection molding technology with which the maximum warpage of a plastic part is greatly reduced. By comparison with the corresponding conventional injection, injecting pressure of the optimized system fluctuates with the same frequency as dynamic flow rate during filling, which plays a significant role for the warpage reduction.

Keywords Dynamic injection molding technology · Warpage optimization · Kriging surrogate model · Expected improvement method · Sequential optimization

X. Wang · J. Gu (✉) · C. Shen · X. Wang
The State Key Laboratory of Structural Analysis for Industrial Equipment, Department of Engineering Mechanics, Dalian University of Technology, Dalian 116023, China
e-mail: jfgu@dlut.edu.cn

1 Introduction

Plastic injection molding products account for more than 50 % in all the plastic products. For most thin-walled components, plastic melt is injected into the cavity by high pressure and solidified in cavity after the cooling process. Plastic material undergoes different temperature fields, stress fields, and density fields during producing a plastic part. This complex process usually causes warpage which may affect the actual utilization of the final products. Therefore, many investigations have focused on the method development about the warpage reduction.

Previous research has made efforts to adjust the conventional process parameters in order to minimize warpage defect. The most important key is to find the optimum manufacturing process conditions. Various mathematical optimization methods combined with the computer-aided engineering (CAE) technology in previous research have been developed for warpage minimization. For instance, Ozcelik and Erzurumlu [1] used design of experiment (DOE) method to select process parameters of interest and employed Taguchi method to obtain the orthogonal parameter arrays. In their work, artificial neural network (ANN) was adopted to evaluate the warpage response value as a predictor of implicit warpage function. Finally, warpage was reduced successfully by genetic algorithm (GA)-based optimization method. Gao and Wang [2] developed an efficient adaptive optimization method on minimizing warpage defect. In contrast to Ozcelik's method, a surrogate model, named Kriging model, is used to represent the warpage response surface in their work. This study implied that the reason of warpage is complicated since each process parameter may affect the warpage of thin-walled plastic part. Moreover, Farshi et al. [3] adopted the sequential variable-size simplex algorithm to minimize both the warpage and the volumetric shrinkage. Deng et al. [4] chose multiclass design variables, which consist of process

parameters, gate location, and geometrical thickness, to optimize multiobjectives including warpage, weld line, and air traps by using particle swarm optimization algorithm (PSO). However, their studies are all based on the conventional injection molding process.

As a successful application of vibration on the melted plastic, dynamic molding technology (DMT) was proposed in plastic molding engineering in the middle of twentieth century. Ibar reviewed this melt vibration technology in detail [5]. He stated that DMT can affect the internal stress, eliminate the defects of the product with different vibration generators, and indicated that DMT can be readily applied to injection or extrusion. For dynamic injection molding technology (DIMT), vibrational process conditions have been introduced into filling, packing, and even plasticizing phase. For instance, one of the significant achievements of Qu and his coworkers is that their new electromagnetic dynamic injection molding machine can play a remarkable role in solid conveying, plasticizing, filling, and packing [6–8].

In the recent 20 years, more and more research have attempted to use DIMT to study the influence of auxiliary vibration on the mechanical or electronic properties of polymer from the experimental perspective. Kikuchi et al. found that the mechanical strength can be enhanced with the help of this vibrational technique [9]. Additionally, they observed that the residual stress distribution of the injected samples can be altered by vibration from the birefringence pattern. Yan et al. found that the shear stress and apparent viscosity were reduced by means of imposing vibration into injection molding [10]. Yang et al. employed DIMT to study the electrical conductivity of the carbon nanotube/polypropylene composite [11]. They indicated that the perfect conductivity paths created in the composite under vibration improve the electrical conductivity.

More devices or apparatus for generating vibration force fields with different vibrational frequencies and locations have been invented [12–16]. However, these papers above focused on studying the properties of material under vibrational process. Few investigations involved warpage analysis of plastic products and the relevant optimization work. Thus, it is necessary to make efforts for warpage reduction by using DIMT.

The aims of this paper are to study the influence of DIMT from the numerical perspective and to perform warpage optimization under DIMT. In this paper, the basic theories for injection molding analysis are presented in Sect. 2.1. Several implementation methods of the dynamic filling and packing are suggested in Sect. 2.2. Subsequently, the surrogate-based sequential searching method is introduced in Sect. 3. Simultaneously, the optimization model on warpage with respect to 12 dynamic injection process parameters is proposed in Sect. 3.3. The optimization results and discussion of a typical component, of which the material and model information are given in Sect. 4, are stated in Sect. 5. The final section is the conclusion about this paper.

2 Numerical dynamic injection molding technology

2.1 The basic governing equations

The classic governing equations to solve the flow of the plastic melt are Eq. (1)~Eq. (3)

$$\frac{1}{\rho}\left(\frac{\partial \rho}{\partial t}+\mathbf{u}\cdot\nabla\rho\right)+\nabla\cdot\mathbf{u}=0 \tag{1}$$

$$\rho\left(\frac{\partial \mathbf{u}}{\partial t}+\mathbf{u}\cdot\nabla\mathbf{u}\right)=\nabla\cdot\boldsymbol{\sigma}+\rho\cdot\mathbf{F} \tag{2}$$

$$\rho c_p\left(\frac{\partial T}{\partial t}+\mathbf{u}\cdot\nabla T\right)=\beta T\left(\frac{\partial p_e}{\partial t}+\mathbf{u}\cdot\nabla p_e\right)+\kappa\cdot(\nabla\cdot\mathbf{u})^2+\boldsymbol{\tau}:\nabla\mathbf{u}+\nabla\cdot(k\nabla T)\quad+\rho\dot{q} \tag{3}$$

where ρ is the density. $\boldsymbol{u}$ and $\boldsymbol{F}$ represent the velocity and body force per unit mass, respectively. c_p, β, and k are the specific heat, coefficient of thermal expansion, and thermal conductivity, respectively. $\dot{q}$ is the heat generation rate per unit mass. κ is the *expansion viscosity*. t, T, and p_e represent the time, temperature, and equilibrium pressure. $\boldsymbol{\sigma}$ is the stress tensor acting on the surface of the material unit which can be decomposed into an isotropic part and a nonisotropic part

$$\boldsymbol{\sigma}=-p\mathbf{I}+\boldsymbol{\tau} \tag{4}$$

where p is the pressure, and $\boldsymbol{I}$ is the identity matrix. $\boldsymbol{\tau}$ is the nonisotropic deviatoric stress tensor, which makes contribution to the internal energy in the form of dissipation of mechanical energy per unit mass in Eq. (3).

Although the plastic melt presents a certain viscoelastic rheological property, it is efficient to regard the plastic melt as the generalized newtonian fluid in the injection molding analysis. The constitutive equation reads as

$$\boldsymbol{\tau}=\eta\left(T,p,\dot{\gamma}\right)\cdot\dot{\boldsymbol{\gamma}} \tag{5}$$

Viscosity $\eta(T,p,\dot{\gamma})$ involves two state parameters, T and p, and follows a nonlinear relationship with respect to shear rate $\dot{\gamma}$. The value of $\dot{\gamma}$ is $\sqrt{(\dot{\boldsymbol{\gamma}}:\dot{\boldsymbol{\gamma}})}/2$ where $\dot{\boldsymbol{\gamma}}$ equals $\nabla\mathbf{u}+\nabla\mathbf{u}^T$. The most commonly used expression of

viscosity is the Williams, Landel, and Ferry (WLF) type of cross model (Eq. (6)) which accords well with the experimental data [17, 18].

$$\eta\left(T,p,\dot{\gamma}\right)=\frac{\eta_0(T,p)}{1+\left[\frac{\eta_0(T,p)}{\tau^*}\dot{\gamma}\right]^{1-n}} \tag{6}$$

where n is the constant named as non-newtonian index. τ^* is a typical stress at which shear thinning happens.

$$\eta_0(T,p)=D_1\cdot\exp\left[-\frac{A_1(T-T^*)}{A_2+(T-T^*)}\right] \tag{7}$$

$$T^*=D_2+D_3\cdot p \tag{8}$$

$$A_2=\overline{A}_2+D_3\cdot p \tag{9}$$

where D_1, D_2, D_3, A_1, and $\bar{A}_2$ are five constants.

2.2 Finite element equation for filling and packing

Pressure field needs to be solved in filling and packing analysis. For the single gate case, the finite element equation for solving pressure field of the current n nodes occupied by melt is

$$\begin{bmatrix} k_{1,1} & k_{1,2} & \cdots & k_{1,l} & \cdots & k_{1,n} \\ k_{2,1} & k_{2,2} & \cdots & k_{2,l} & \cdots & k_{2,n} \\ \vdots & \vdots & \cdots & \vdots & \cdots & \vdots \\ k_{l,1} & k_{l,2} & \cdots & k_{l,l} & \cdots & k_{l,n} \\ k_{l+1,1} & k_{l+1,2} & \cdots & k_{l+1,l} & \cdots & k_{l+1,n} \\ \vdots & \vdots & \cdots & \vdots & \cdots & \vdots \\ k_{n,1} & k_{n,2} & \cdots & k_{n,l} & \cdots & k_{n,n} \end{bmatrix}\begin{bmatrix} P_g \\ P_2 \\ \vdots \\ P_l \\ 0 \\ \vdots \\ 0 \end{bmatrix}=\begin{bmatrix} Q_g \\ 0 \\ \vdots \\ 0 \\ Q_{l+1} \\ \vdots \\ Q_n \end{bmatrix} \tag{10}$$

where $k_{i,j}$ is the stiffness. P_{index} is the node pressure. A nonzero value of P_{index} indicates that the *index* node is the internal node, and zero pressure means that the *index* node is the forefront node. When the subscript index is g, it means that the g node is the injecting gate. Q_{index} in the right hand side represents the net flow rate of the *index* node.

For filling analysis, Q_g is the given boundary condition of gate, whereas the pressure field needs to be solved by over-relaxation iterative method. On the contrary, P_g is designated in the subsequent packing analysis and Q_{index} is unknown. In traditional injection molding analysis, these given boundary conditions are usually constant values or linear functions. For instance, the velocity of the screw and the packing pressure curve are usually linear functions with respect to time.

2.3 Realizations of the numerical DIMT

The early DMT mainly takes the square wave vibration, as shown in Fig. 1, since the motivation of injection machinery comes from the hydraumatic which can be readily imposed into the producing process of plastic components. It can take the sawtooth wave vibration (Fig. 2) as well. Thus, these two noncontinuous pulse vibration forms can be employed as the dynamic filling flow rate $Q(t)$. However, this type of injection machine is gradually substituted by all-electric injection machine.

Another technique to carry out dynamic filling comes from the continuous advancing displacement function (Eq. (11)) of the screw with respect to time

$$S(t)=v_{ave}\cdot t+S_{amp}\cdot\sin\left(2\pi f_{fill}\cdot t+\varphi_{fill}\right) \tag{11}$$

where v_{ave} is the average advancing velocity. S_{amp}, f_{fill}, and φ_{fill} are amplitude, frequency, and initial phase of the dynamic advancing displacement of the screw, respectively.

The dynamic flow rate derives from computing the derivative of $S(t)$ with respect to time t as Eq. (12). This dynamic injection process has been proved to be feasible by Yin et al. [19].

$$\begin{aligned} Q(t)&=Av_{ave}\left[1+\upsilon\cdot\cos\left(2\pi f_{fill}\cdot t+\varphi_{fill}\right)\right] \\ &=\frac{V}{t_{fill}}\cdot\left[1+\upsilon\cdot\cos\left(2\pi f_{fill}\cdot t+\varphi_{fill}\right)\right] \end{aligned} \tag{12}$$

where A is the area of the screw. V is the total volume of the object to be filled. t_{fill} is the total filling time. υ equals (S_{amp} 2-π f_{fill} t_{fill} A)/V which is regarded as a factor of the vibrational amplitude of flow rate.

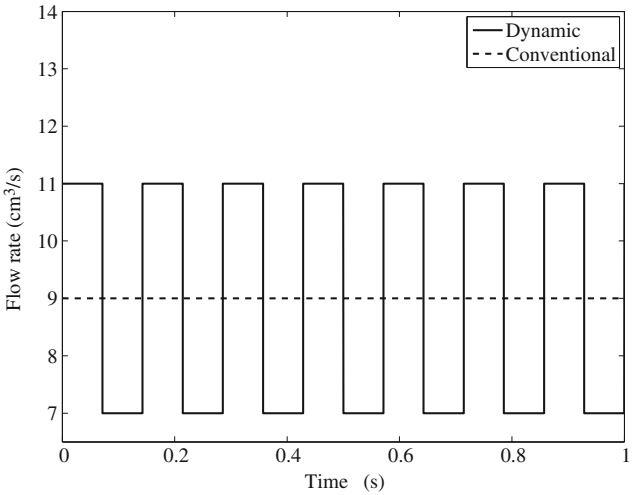

Fig. 1 The square wave flow rate

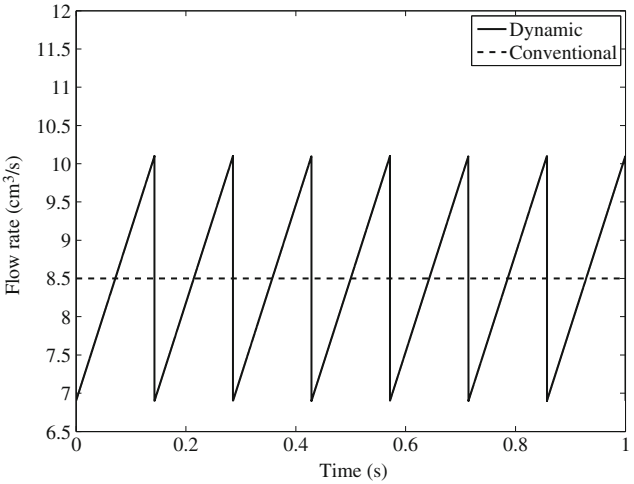

Fig. 2 The sawtooth wave flow rate

Another analogous dynamic flow rate (Eq. (14)) directly comes from the dynamic advancing velocity (Eq. (13)).

$$v(t) = v_{ave}\left[1 + \varepsilon \cdot \sin\left(2\pi f_{fill} \cdot t + \varphi_{fill}\right)\right] \tag{13}$$

$$Q(t) = \frac{V}{t_{fill}}\left[1 + \varepsilon \cdot \sin\left(2\pi f_{fill} \cdot t + \varphi_{fill}\right)\right] \tag{14}$$

where ε is the amplitude factor.

Equation (12) and Eq. (14) are both available for dynamic filling. Figure 3 presents the difference between them. It is worth to note that the amplitude factor ε in Eq. (14) is an independent parameter, whereas υ is greatly affected by three process parameters S_{amp}, f_{fill}, and t_{fill} from its definition. This dependence between parameters implies a constraint that in order to guarantee no melt reflux, $S_{amp}\ 2\pi\ f_{fill}\ \ t_{fill}\ A \leq V$ has to be satisfied in Eq. (12). It means that high frequency will result in extremely low amplitude S_{amp} due to this constraint, especially for the ultrasonic vibration. When S_{amp} is extremely low, this dynamic injection will make no sense in practice because Eq. (11) yields conventional configuration. On the other hand, this constraint will make the optimization work more complicated. Therefore, we prefer to use Eq. (14) rather than Eq. (12) in the following sections. Additionally, if ε or f_{fill} is zero in Eq. (14), dynamic filling will be transformed into the conventional filling with constant flow rate.

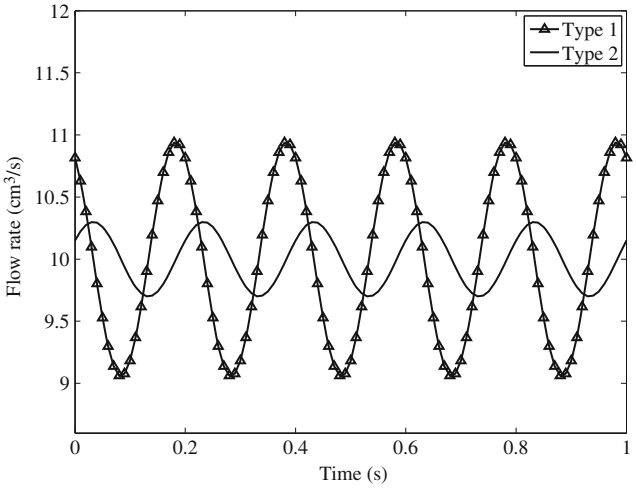

Fig. 3 Two types of flow rate curve: Type 1 derives from Eq. (12) where S_{amp} equals 0.03 mm and type 2 derives from Eq. (14) where ε equals 0.03. Frequency and phase of these two types are equal

$$Q(t) = Q_0 + k \cdot t + \varepsilon \cdot \sin\left(2\pi f_{fill} \cdot t + \varphi_{fill}\right) \tag{15}$$

More equations may be taken into account. For example, Fig. 4 shows another more complex piecewise linear function for dynamic filling. In each piece of this flow rate, Eq. (15) is used. The amplitude and frequency of this process condition can adopt different values in each piece, and the total number of the vibrational parameters will be much more than that in Eq. (14).

In packing phase, the dynamic packing pressure can be simply defined as Eq. (16). We choose Eq. (17) as the dynamic packing pressure since the packing pressure should be decreasing sometimes.

$$P_{packing} = P_{finalP} \cdot \left[P_{start} + \xi \cdot \sin\left(2\pi f_{pack} \cdot t + \varphi_{pack}\right)\right] \tag{16}$$

$$P_{packing} = P_{finalP} \cdot \left[(P_{start} - \delta \cdot t) + \xi \cdot \sin\left(2\pi f_{pack} \cdot t + \varphi_{pack}\right)\right] \tag{17}$$

where P_{finalP} is the final filling pressure obtained at the end of filling process. P_{start} denotes the initial pressure fraction. δ can describe the total tendency of the packing pressure curve. A

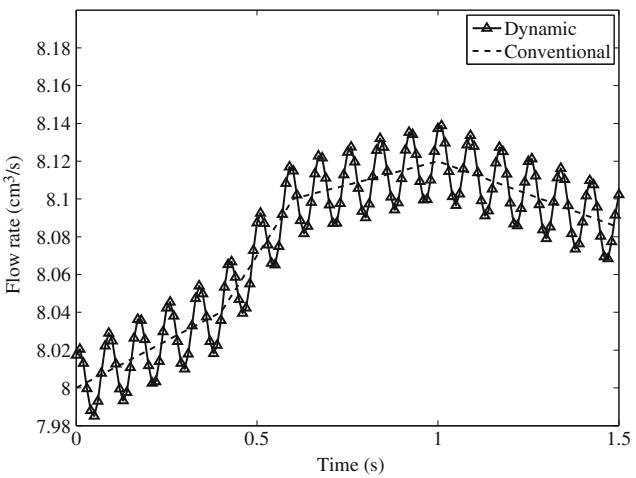

Fig. 4 A case of the piecewise dynamic flow rate and the corresponding conventional case

large positive δ gives a fast decreasing packing pressure. ξ, f_{pack}, and φ_{pack} are the amplitude factor, frequency, and phase in dynamic packing process, respectively. If ξ or f_{pack} is zero, dynamic packing turns to be a conventional linear packing. Furthermore, if δ equals zero too, packing pressure becomes to be the constant form.

This new dynamic packing pressure can be defined more complicated as well. However, these measures will result in a more high-dimensional optimization problem which may be difficult to search the optimum results. The detail investigation about these complex molding conditions in filling and packing will be our future work.

As an application example of DIMT, a LDPE disk is used to study the dynamic pressure response. Four locations are monitored in this model as flagged in Fig. 5a. It is obvious that the dynamic flow rate induces different fluctuating levels to the node pressure. This remarkable influence depends on the distance between the node of interest and the gate. It says that the vibration can propagate from the gate to a certain distance and affects the mechanical quantities, such as pressure and shear stress. The pressure response of the gate is similar with the experimental observation of Yin et al. [19], although their research adopted Eq. (11) as the injection condition. This similarity can be clarified from the definitions of the flow rate. However, Eq. (14) has certain advantages as we have mentioned above.

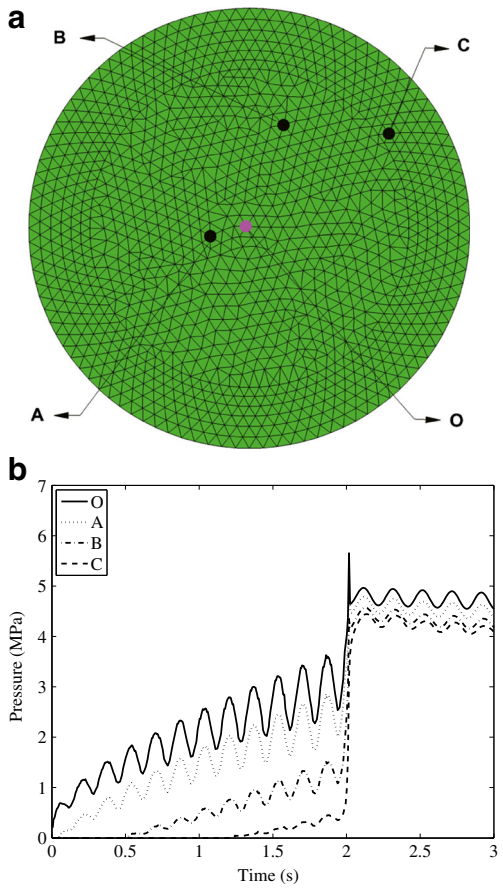

Fig. 5 A LDPE disk model (**a**) and the pressure response curve of four locations (**b**): *O* is the gate; R_{AO}=10.08 mm; R_{BO}=29.40 mm; R_{CO}=46.34 mm. **a** LDPE disk model. **b** Pressure response curve

3 Expected improvement-based sequential optimization method

3.1 Preliminary knowledge of Kriging surrogate model

Commonly, the relationship between the objective and design parameters in engineering optimization problem is implicit or "black." Numerous surrogate models are studied to address this "black function" in order to give a good prediction to the real problem [20–22]. As one of these methods, Kriging model is regarded as the *best linear unbiased predictor* (BLUP) [23]. Thus, Kriging model is employed as the substitute for the objective in many optimization problems. For instance, Jouhaud et al. used the ordinary Kriging model to evaluate the cost function in the two-dimensional shape optimization of a wing which suffered turbulent flow with low-Reynolds, incompressible conditions [24]. Sun et al. used Kriging surrogate model to deal with the implicit robust objective and constraints in the robust optimization of a foam-filled thin-walled structures under impact [25].

Kriging model (Eq. (18)) is composed of a linear regression part and an error term $e(\boldsymbol{x})$. The regression part determines the order of the Kriging model and gives the main prediction, while the error term provides the local modification.

$$y(\mathbf{x}) = \sum_{l=1}^{p} \beta_l f_l(\mathbf{x}) + e(\mathbf{x}) \tag{18}$$

where β_l and $f_l(\boldsymbol{x})$ are the l_{th} regression coefficient and polynomial, respectively.

In addition, $e(\boldsymbol{x})$ follows $norm[0, \sigma_e^2]$ with respect to the m-dimensional design variables $\boldsymbol{x}$. $e(\boldsymbol{x}_i)$ and $e(\boldsymbol{x}_j)$ are assumed to be correlated about the spatial weighted distance (Eq. (19)). Therefore, Kriging model presents the stochastic property due to the error term and provides the postdistribution of the prediction with the aid of n given design points $\boldsymbol{X}=\{\boldsymbol{x}_1, \boldsymbol{x}_2, \ldots, \boldsymbol{x}_n\}$ and the corresponding response $\boldsymbol{Y}=\{y_1, y_2, \ldots y_n\}$.

$$\begin{aligned} Cov\left[e(\mathbf{x}_i), e(\mathbf{x}_j)\right] &= \sigma_e^2 \cdot R_{ij}(\boldsymbol{\theta}, \mathbf{x}_i, \mathbf{x}_j) \\ &= \sigma_e^2 \cdot \prod_{k=1}^{m} \exp\left[-\theta_k \left(x_i^k - x_j^k\right)^2\right] \end{aligned} \tag{19}$$

where σ_e^2 is the variance of $e(\boldsymbol{x})$. R_{ij} is the correlation function employed in the *Gaussian* type here. θ_k is the k_{th}-dimensional correlated coefficient.

The critical issue for constructing a Kriging model is to estimate the parameters $\boldsymbol{\beta}$, $\boldsymbol{\theta}$, and σ_e^2. Jerome [26] and Gao [2] have demonstrated the procedure to attain these estimators in detail. The derivatives of the likelihood function Eq. (20) result in two estimators of $\boldsymbol{\beta}$ and σ_e^2. The remained $\boldsymbol{\theta}$ will be determined by optimizing the following equivalent problem Eq. (23).

$$\frac{1}{\left(2\pi\sigma_e^2\right)^{n/2}|\mathbf{R}|^{1/2}}\exp\left[-\frac{\left(\mathbf{Y}-\mathbf{F}^T\boldsymbol{\beta}\right)^T\mathbf{R}^{-1}\left(\mathbf{Y}-\mathbf{F}^T\boldsymbol{\beta}\right)}{2\sigma_e^2}\right] \tag{20}$$

$$\widetilde{\boldsymbol{\beta}}=\left(\mathbf{F}^T\mathbf{R}^{-1}\mathbf{F}\right)^{-1}\cdot\mathbf{F}^T\mathbf{R}^{-1}\mathbf{Y} \tag{21}$$

$$\widetilde{\sigma}_e^2=\frac{1}{n}\left(\mathbf{Y}-\mathbf{F}^T\widetilde{\boldsymbol{\beta}}\right)^T\mathbf{R}^{-1}\left(\mathbf{Y}-\mathbf{F}^T\widetilde{\boldsymbol{\beta}}\right) \tag{22}$$

$$\widetilde{\boldsymbol{\theta}}=\min\left\{|\mathbf{R}|^{1/n}\widetilde{\sigma}_e^2\right\} \tag{23}$$

where $\boldsymbol{R}$ and $\boldsymbol{F}$ are the correlation matrix and polynomial matrix, respectively. The order of the Kriging model is determined by the polynomial matrix $\boldsymbol{F}$. For the ordinary Kriging (OK) model, $\boldsymbol{F}$ yields a vector $\boldsymbol{l}$ in which l_i= 1.

This paper chooses the ordinary Kriging model since it is commonly used and efficient enough for most investigations in practice. The corresponding expectation and variance of the postprediction are written as Eq. (24) and Eq. (25), respectively.

$$\overline{y}(\mathbf{x})=\widetilde{\mu}+\mathbf{r}^T\mathbf{R}^{-1}\left(\mathbf{Y}-\widetilde{\mu}\mathbf{l}\right) \tag{24}$$

$$\widetilde{s}^2(\mathbf{x})=\widetilde{\sigma}_e^2\left[1+\left(\mathbf{l}^T\mathbf{R}^{-1}\mathbf{l}\right)^{-1}\left(1-\mathbf{l}^T\mathbf{R}^{-1}\mathbf{r}\right)^2-\mathbf{r}^T\mathbf{R}^{-1}\mathbf{r}\right] \tag{25}$$

where $\widetilde{\mu}=\left(\mathbf{l}^T\mathbf{R}^{-1}\mathbf{l}\right)^{-1}\left(\mathbf{l}^T\mathbf{R}^{-1}\mathbf{Y}\right)$. l_i=1; $r_i=R\left(\widetilde{\boldsymbol{\theta}},\mathbf{x},\mathbf{x}_i\right)$.

3.2 Expected improvement function

The Kriging surrogate model greatly depends on the number and spatial distribution of the given sample points; so, direct optimization on this surrogate model of engineering problem is not suitable. Especially for high dimensional engineering optimization problem, the implicit objective function is usually highly nonlinear. Kriging model provides the predicting information at any design point, $\overline{y}(\mathbf{x})$ and $\widetilde{s}^2(\mathbf{x})$. In expected improvement (EI)-based sequential optimization method, a variable $I(\mathbf{x})$ named improvement is defined as $max[0, y_{min}\text{-}y(\boldsymbol{x})]$. The aim of improvement is searching for the design point whose response value is better than the current best one y_{min} in the given samples. $I(\boldsymbol{x})$ also has the properties of *Gaussian* process. The probability density function of $I(\boldsymbol{x})$ follows

$$p[I(\mathbf{x})]=\frac{1}{\sqrt{2\pi}\widetilde{s}(\mathbf{x})}\exp\left\{-\frac{\left[I(\mathbf{x})-\left(y_{\min}-\overline{y}(\mathbf{x})\right)\right]^2}{2\widetilde{s}^2(\mathbf{x})}\right\} \tag{26}$$

EI function is the expectation of $I(\boldsymbol{x})$ derived by

$$\begin{aligned}E[I(\mathbf{x})]&=\int_0^{+\infty}I'(\mathbf{x})\cdot p[I(\mathbf{x})]\;dI'(\mathbf{x})\\&=\widetilde{s}(\mathbf{x})\phi\left[\frac{y_{\min}-\overline{y}(\mathbf{x})}{\widetilde{s}(\mathbf{x})}\right]+[y_{\min}-\overline{y}(\mathbf{x})]\Phi\left[\frac{y_{\min}-\overline{y}(\mathbf{x})}{\widetilde{s}(\mathbf{x})}\right]\end{aligned} \tag{27}$$

where ϕ and Φ are the standard normal density function and distribution function, respectively.

Jones found the monotonicity of EI function with respect to $\overline{y}(\mathbf{x})$ and $\widetilde{s}^2(\mathbf{x})$ [27]. Two concise formulas Eq. (28) and Eq. (29) give the explanations on the importance of the *maximum expected improvement* (MEI) value. The MEI value is either located at a point better than y_{min} or the most imprecise point in the current Kriging model. The MEI point is usually not the optimum solution of the original problem. However, it gives us a feasible and meaningful design point as a guide to refine the current Kriging model. EI-based optimizing process is a global searching and sequential revising process. The optimal design point is obtained during this process. Therefore, EI-based optimization method is acknowledged as the *efficient global optimization method* (EGOM) by some researchers [25].

$$\frac{\partial E[I(\mathbf{x})]}{\partial\overline{y}(\mathbf{x})}=-\Phi\left[\frac{y_{\min}-\overline{y}(\mathbf{x})}{\widetilde{s}(\mathbf{x})}\right]\le 0 \tag{28}$$

$$\frac{\partial E[I(\mathbf{x})]}{\partial\widetilde{s}(\mathbf{x})}=\phi\left[\frac{y_{\min}-\overline{y}(\mathbf{x})}{\widetilde{s}(\mathbf{x})}\right]\ge 0 \tag{29}$$

3.3 EI-based warpage optimization

EI-based sequential optimization method is general for any engineering optimization problem. In the following warpage optimization problem of dynamic injection molding, design parameters involve melt temperature T_{melt} (x^1), wall temperature T_{wall} (x^2), filling time t_{fill} (x^3), packing time t_{pack} (x^4), initial packing pressure fraction P_{start} (x^5), tendency coefficient δ (x^6), amplitude factor ε (x^7), frequency f_{fill} (x^8), and phase φ_{fill} (x^9) of the dynamic filling flow rate, amplitude factor ξ (x^{10}), frequency f_{pack} (x^{11}), and phase φ_{pack} (x^{12}) of the dynamic packing pressure.

Optimization model is

$$\begin{array}{ll} \text{Find} & \boldsymbol{x} = \left[x^1, x^2, x^3, \ldots, x^{12}\right] \\ \text{Minimize} & Obj(\mathbf{x}) = warpage(\mathbf{x}) \\ \text{Subjected to} & x^i_{lb} \le x^i \le x^i_{ub}, x^i \in \mathbf{x} \;\; i = 1, 2 \ldots \;\; 12 \end{array} \tag{30}$$

where x^i is the i_{th} variable in the parameter set $\boldsymbol{x}$; x^i_{lb} and x^i_{ub} are the lower and upper bound of the i_{th} variable as listed in Table 1.

Procedure of the sequential searching process for the warpage optimization follows the steps below:

(a) Create the initial samples about the maximum total warpage in the plastic part;
(b) Construct Kriging model of the maximum warpage with the given samples;
(c) Search the MEI point with the aid of GA;
(d) Judge the criterion of convergence. If not, add the current point into the sample set and rebuilt the model until criterion is satisfied.

4 Model, material, and optimization model

As a simulation application, a cellular phone cover model including 2059 nodes and 3732 triangle elements is taken into account. Length, width, height, and thickness of this model are 129.8, 55.25, 12, and 1.5 mm, respectively. Injecting gate locates at the red position in Fig. 6.

Molding material is the compound of polycarbonate (PC) and acrylonitrile-butadiene-styrene (ABS) produced by Teijin Chemicals Company. Density of melt and solid of PC/ABS are 1.1092 and 1.2038 g/cm^3, respectively. Thermal conductivity is 0.294 W/m°C. Elastic module, Poisson ratio, and transform temperature of this material are 2780 MPa, 0.4 and 104 °C, respectively.

5 Results and discussions

The maximum warpage deformation of the simulation model in Fig. 7a is 0.094 mm by using the previous EI-based sequential optimization method. This value is less than that of the best sample (0.131 mm in Fig. 7b) with about 28.24 % warpage reduction. Compared with case 1 (0.282 mm in Fig. 7c) which only takes six conventional parameters of the 12 optimized parameters for warpage analysis as shown in Table 2, the optimization result is reduced by 66.67 %. It means that dynamic injection can reduce warpage than conventional injection. This optimization result is clarified to be reasonable, as shown in Fig. 8, by changing one of the 12 parameters from lower bound to upper bound and keeping others invariant simultaneously.

Note that two parameters x^6 (δ) and x^{10} (ξ) achieve the boundary values. In Sect. 2, δ is defined as the decreasing ratio of the packing pressure. The values of δ and ξ rely on the initial packing pressure $P^{initial}_{Pack}$. When $P^{initial}_{Pack}$ is large enough, packing pressure should decrease fast and steady to release the internal pressure with larger δ and lower ξ to avoid overpacking. In practice, packing pressure should decrease slowly, even increase, to compensate extra material and keep from unacceptable shrinkage.

There is an issue on the optimization result that when ξ is zero, the dynamic packing process yields the conventional packing. The number of the "optimal result" will be countless in mathematics since packing frequency and phase can take any value and will not affect the warpage anymore as shown in the last two subfigures of Fig. 8.

Actually, engineering optimization problem is usually highly nonlinear in high-dimensional design space. Since the complexity of warpage response surface is not clear, the real global optimal solution in mathematics is usually unknown in terms of value and the number. However, the EI-based sequential optimization method has a good global searching ability, and the significance of this optimization work is to search a set of process parameters better than the best one we have attained.

Warpage results relate to injection history. In filling phase, the solution of the pressure filed depends on the inlet flow rate. For dynamic filling, flow rate is composed of a mean value and a harmonic part. A lower (higher) flow rate than the mean value will cause a lower (higher) injecting pressure than the conventional filling. It leads to three phenomena. First of all, injecting pressure of the gate and internal nodes of the dynamic case fluctuates near the conventional injection pressure curve as time proceeds. Second, the fluctuating frequency of the dynamic injecting pressure is the same as flow rate as shown in Fig. 9a. The same thing happens to the frequency of the injecting pressure difference (Fig. 9b) between the dynamic case and the corresponding conventional case. The last one

Table 1 The boundary values of the design parameters

	Design parameters											
	x^1	x^2	x^3	x^4	x^5	x^6	x^7	x^8	x^9	x^{10}	x^{11}	x^{12}
Lower	230	50	0.2	0.5	60	0	0	0	0	0	0	0
Upper	300	92	1	5	90	10	1	20	2π	30	50	2π

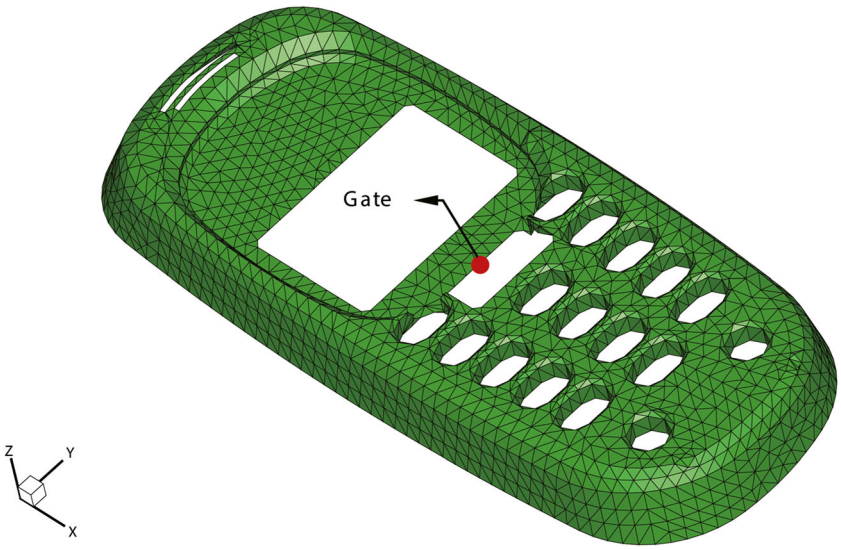

Fig. 6 The cellular phone cover model for investigation

is that the fluctuating amplitude increases with time because injecting pressure also depends on flow length. These aspects not only result in different injecting histories but also influence the calculation of the temperature field.

In packing phase, it is reasonable that the packing pressure of case 1 is a little lower than the dynamic case with the same trend. The reason is that the final filling pressure value of the dynamic case is different from the conventional case due to vibrational filling. Generally speaking, the impact of packing history on warpage is not negligible. Thus, the authors have finished another warpage analysis (case 2) of which the warpage contour is shown in Fig. 7d and the injecting pressure history is presented in Fig. 10. Case 2 has the same filling history as case 1 by taking the same conventional molding parameters, and the same packing history as the optimization result by employing the same initial packing pressure in Table 3. This analysis results indicate that this difference of packing pressure between the optimization result and case 1

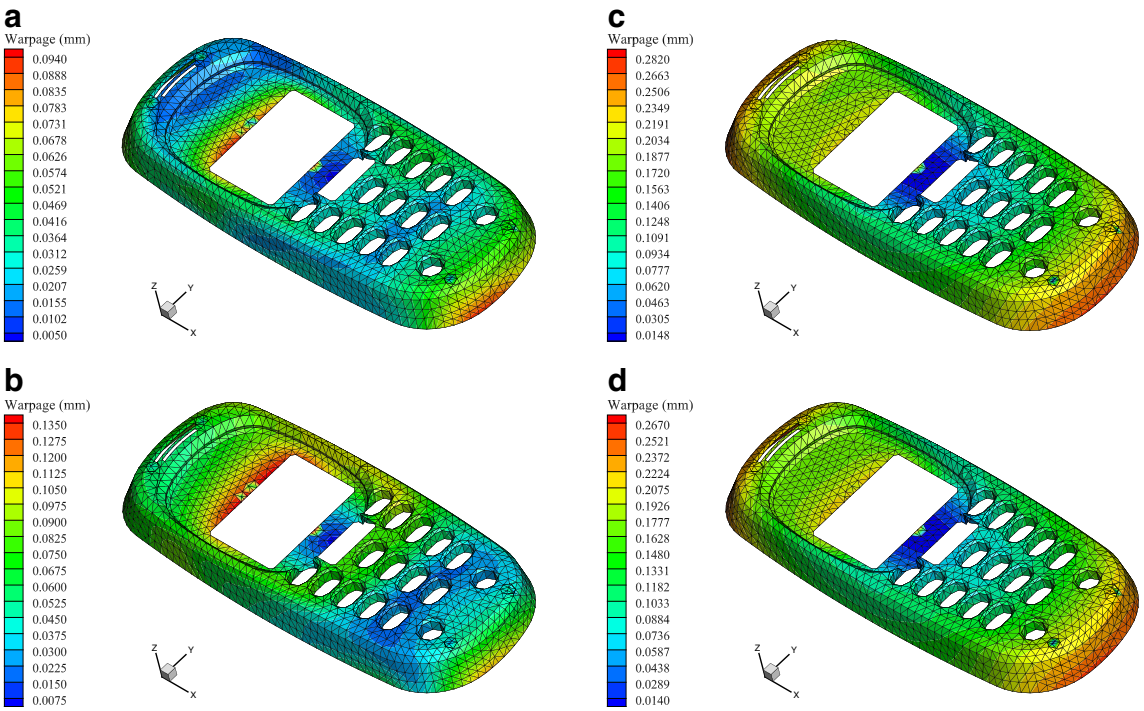

Fig. 7 Warpage contour of the cellular phone cover model: **a** optimization result; **b** best in initial samples; **c** case 1 which only takes the conventional parameters of the optimization result listed in Table 2; **d** case 2 which takes the same parameters as case 1, but is imposed to have the same initial packing pressure as the optimization result listed in Table 3

Table 2 Parameters and the warpage results of the phone cover

	Design parameters												Objective
	x^1	x^2	x^3	x^4	x^5	x^6	x^7	x^8	x^9	x^{10}	x^{11}	x^{12}	Warpage(mm)
Before optimization	262.43	74.71	0.96	1.95	84.41	7.55	0.64	0.59	0.13	3.63	24.41	5.73	0.131
Optimization result	277.82	77.06	0.72	3.31	82.86	10.00	0.32	11.39	1.67	0.00	48.74	1.74	0.094
Case 1	277.82	77.06	0.72	3.31	82.86	10.00	0.00	0.00	0.00	0.00	0.00	0.00	0.282

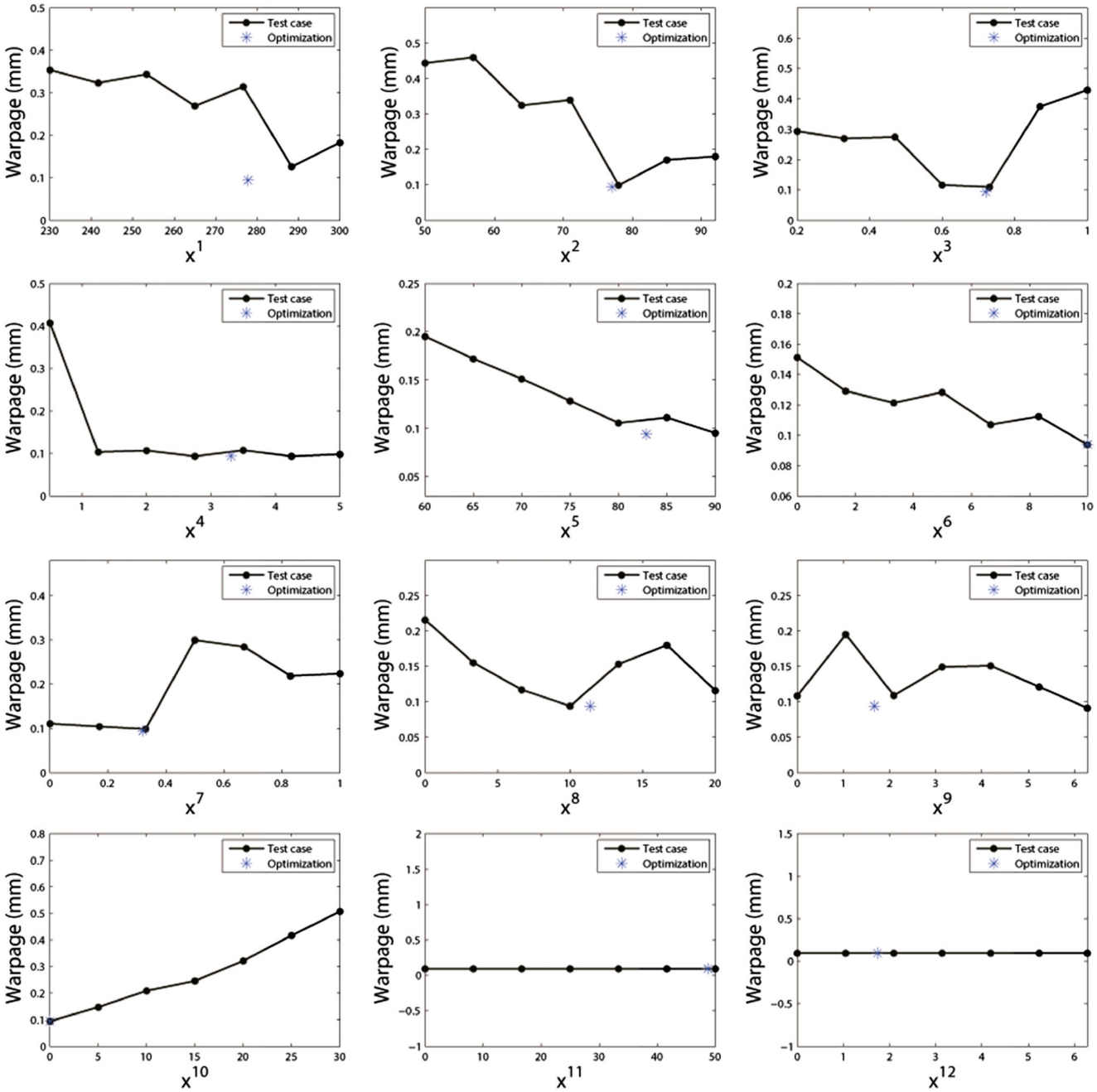

Fig. 8 Effect of each process parameter on warpage (test case in subfigures represents the case that only x^i in the optimization result is changed to perform warpage analysis from lower bound to upper bound)

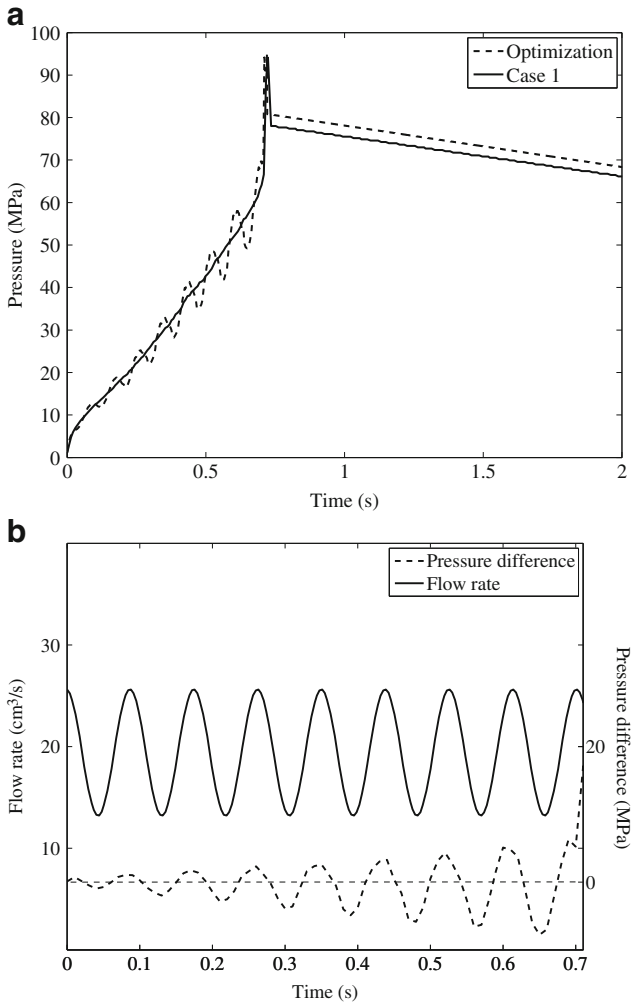

Fig. 9 Pressure response of the optimization result and case 1. Subfigure **a** is the injecting pressure; subfigure **b** is the pressure difference between these two cases in filling

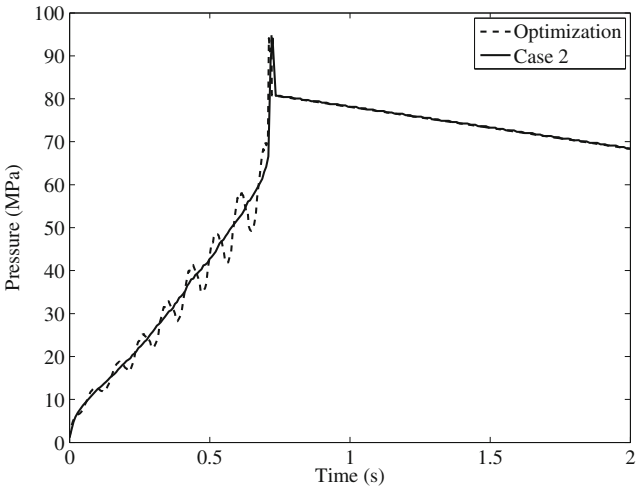

Fig. 10 Pressure response of the optimization result and case 2

Table 3 Warpage comparison between the optimization result, case 1 and case 2

	$P_{Pack}^{initial}(MPa)$	Warpage(mm)
Optimization result	80.83	0.094
Case 1	77.99	0.282
Case 2	80.83	0.267

has slight effect on warpage. Namely, dynamic filling has remarkable influence on the consequent analysis of packing and warpage for this simulation.

Overall, this optimization result suggests an argument that DIMT can improve the quality of the plastic part than the conventional.

6 Conclusion

This paper introduces several measures to realize the numerical dynamic filling and packing. The injecting pressure response exhibits interesting characteristics and is consistent with the observation in experiment. Based on a simple harmonic dynamic injection molding process, warpage optimization is performed on a cell phone cover.

In this optimization, Kriging surrogate model is used as an evaluator of the warpage response surface with respect to 12 process parameters. Then, EI-based method associated with GA is employed to perform the warpage optimization. The optimization result indicates that the DIMT can reduce the maximum warpage of the injected component. The study about the effect of individual parameter on warpage supports the optimization result. The Kriging surrogate model and EI-based sequential optimization method efficiently deal with this 12 dimensions engineering optimization problem.

More complex dynamic filling and packing conditions can be further studied, and another important issue that the mechanism of reducing the maximum warpage with the dynamic process condition needs to be investigated deeply. Moreover, DIMT makes a vibrational force field which exerts on the microstructure of polymer. The evolution of the microstructure under this force filed, e.g., disentanglement of micromolecular chain which cause the high viscosity of the melt, is also an interesting and meaningful work to be investigated.

Acknowledgments The authors would like to acknowledge financial support gratefully for this work from the National Basic Research Program of China (No. 2012CB025905), the National Natural Science Funds of China (No. 11202049), the 111 Project (B14013) and the Fundamental Research Funds for the Central Universities, and thank National Engineering Research Center of Advance Polymer Processing Technology of Zhengzhou University of China for the supporting of the simulation software.

References

1. Ozcelik B, Erzurumlu T (2006) Comparison of the warpage optimization in the plastic injection molding using ANOVA, neural network model and genetic algorithm. J Mater Process Tech 171(3):437–445
2. Gao YH, Wang XC (2008) An effective warpage optimization method in injection molding based on the Kriging model. Int J Adv Manuf Technol 37(9–10):953–960
3. Farshi B, Gheshmi S, Miandoabchi E (2011) Optimization of injection molding process parameters using sequential simplex algorithm. Mater Design 32(1):414–423
4. Deng YM, Zheng D, Lu XJ (2008) Injection moulding optimisation of multi-class design variables using a PSO algorithm. Int J Adv Manuf Technol 39(7–8):690–698
5. Ibar JP (1998) Control of polymer properties by melt vibration technology: a review. Polym Eng Sci 38(1):1–20
6. Wang Q, Qu JP, Huang CH, Liu B, Sun X (2013) Effect of vibration parameters in plasticizing process on properties of polypropylene by dynamic injection molding. J Thermoplast Compos. doi:10.1177/0892705713513287
7. Wang Q, Qu JP (2006) Mechanical properties and morphological behavior of calcium carbonate-filled polypropylene in dynamic injection molding. Polym Int 55(11):1330–1335
8. Wang Q, Qu JP, He L (2006) Effect of vibration parameters of electromagnetic dynamic plastics injection molding machine on mechanical properties of polypropylene samples. J Appl Polym Sci 102(2):972–976
9. Kikuchi A, Coulter J, Gomatam R (2006) Assessing the effect of processing variables on the mechanical response of polysytrene molded using vibration-assisted injection molding process. J Appl Polym Sci 99(5):2603–2613
10. Yan Z, Shen KZ, Zhang J, Chen LM, Zhou C (2002) Effect of vibration on rheology of polymer melt. J Appl Polym Sci 85(8):1587–1592
11. Yang LB, Liu FH, Xia HS, Qian XY, Shen KZ, Zhang J (2011) Improving the electrical conductivity of a carbon nanotube/polypropylene composite by vibration during injection-moulding. Carbon 49(10):3274–3283
12. Astier JF, Bessaguet L, LaPlanche M (1985) Vibration-aided feed device for a molding apparatus. US Patent 4,500,280, Feb. 19
13. Probst G (1995) Device employing vibration for transporting plastic substances with a high coefficient of friction. US Patent 5,435,712, July 25
14. Ibar JP (1999) Viscosity control for molten plastics prior to molding. US Patent 5,885,495, Mar. 23
15. Qu JP (1999) Polymer's electromagnetic dynamic injection molding method and the apparatus therefor. US Patent 5,951,928, Sep. 14
16. Sato A, Ito H, Koyama K (2009) Study of application of ultrasonic wave to injection molding. Polym Eng Sci 49(4):768–773
17. Williams ML, Landel RF, Ferry JD (1955) The temperature dependence of relaxation mechanisms in amorphous polymers and other glass-forming liquids. J Am Chem Soc 77(14):3701–3707
18. Cross MM (1965) Rheology of non-Newtonian fluids: a new flow equation for pseudoplastic systems. J Colloid Sci 20(5):417–437
19. Yin XC, Zeng WB, He GJ, Yang ZT, Qu JP (2014) Influence of pressure oscillation on injection molding process. J Thermoplast Compos 27(10):1417–1427
20. Deboor C, Ron A (1992) Computational aspects of polynomial interpolation in several variables. Math Comput 58(198):705–727
21. Huang D, Allen TT, Notz WI, Miller RA (2006) Sequential kriging optimization using multiple-fidelity evaluations. Struct Multidiscip Optim 32(5):369–382
22. Kitayama S, Onuki R, Yamazaki K (2014) Warpage reduction with variable pressure profile in plastic injection molding via sequential approximate optimization. Int J Adv Manuf Technol 72(5–8):827–838
23. Cressie N (1990) The origins of kriging. Math Geol 22(3):239–252
24. Jouhaud JC, Sagaut P, Montagnac M, Laurenceau J (2007) A surrogate-model based multidisciplinary shape optimization method with application to a 2D subsonic airfoil. Comput Fluids 36(3):520–529
25. Sun GY, Song XG, Baek S, Li Q (2014) Robust optimization of foam-filled thin-walled structure based on sequential Kriging metamodel. Struct Multidiscip Optim 49(6):897–913
26. Sacks J, Welch WJ, Mitchell TJ, Wynn HP (1989) Design and analysis of computer experiments. Stat Sci 4(4):409–423
27. Jones DR, Schonlau M, Welch WJ (1998) Efficient global optimization of expensive black-box functions. J Glob Optim 13(4):455–492